Eur. Phys. J. B **31**, 179–194 (2003)
DOI: 10.1140/epjb/e2003-00022-x

THE EUROPEAN PHYSICAL JOURNAL B

Fluorescence of a dye-doped cholesteric liquid crystal film in the region of the stop band: theory and experiment

J. Schmidtke[a] and W. Stille

Physikalisches Institut, Albert-Ludwigs-Universität, Hermann-Herder-Str. 3, 79104 Freiburg, Germany

Received 10 September 2002
Published online 4 February 2003 –

Abstract. Due to the sinusoidal modulation of the dielectric properties along the helical axis, cholesteric liquid crystals exhibit a photonic stop band for circularly polarized light, which strongly affects the emission of fluorescent guest molecules. In this paper, we discuss the resulting changes in the emission spectrum. In an analytical treatment, we first derive the photonic densities of states of the two normal light modes for propagation parallel to the helical axis, taking into account multiple reflections due to the finite film thickness. Then we discuss the influence of the degree of order of the dye's transition dipole moment on the emission characteristics. Finally, we present experimental results, which show excellent quantitative agreement with our theoretical description.

PACS. 42.70.Qs Photonic bandgap materials – 61.30.-v Liquid crystals

1 Introduction

Dielectric materials with a periodic modulation of the refractive index exhibit photonic band gaps, *i.e.*, in certain frequency ranges the propagation of light is forbidden. Such optical media are known as photonic crystals. The presence of a photonic band gap affects the emission spectrum of fluorescent guest molecules: inside the gap, fluorescence is suppressed, near the band edges it is enhanced due to the high photonic density of states (DOS); at the band edges, the group velocity approaches zero, and the resulting long dwell times of emitted photons strongly support stimulated emission. Hence, photonic crystals may be used as mirrorless resonators for laser emission.

Cholesteric liquid crystals (CLCs) provide a 1D refractive index modulation: a CLC is a fluid medium consisting of rodlike molecules which arrange themselves in a helical structure [1]. In planes perpendicular to the helical axis, the molecules show a nematic-like order. The preferred orientation of the molecules defines the local optical axis. This direction can be characterized by a unit vector $\hat{\boldsymbol{n}}$, the so-called director. Along the helical axis, the director is continuously rotated, resulting in a twisted birefringent medium. For light propagation along the helical axis, the two normal light modes are elliptically polarized waves with opposite sense of rotation [2]. In a certain frequency range, a CLC shows a stop band for that mode whose polarization has the same sense of rotation as the cholesteric helix. Thus, CLCs may be regarded as self-assembling 1D photonic crystals.

[a] e-mail: juergen.schmidtke@physik.uni-freiburg.de

Indeed it has been repeatedly demonstrated, that dye-doped low molar mass CLCs [3–6] as well as cholesteric polymer networks [7,8] act as photonic band edge lasers. As a prerequisite for a thorough understanding of the observed lasing phenomena, one has to understand the effect of the cholesteric medium on the spontaneous emission of the dye molecules. On transition from the isotropic to the cholesteric phase, there are strong changes in the fluorescence spectrum: reduced emission inside the stop band, enhanced emission at the band edges, and (at least in well ordered films) the occurrence of Fabry-Perot-like oscillations [8]. Besides, one observes a dominant circularly polarized emission component near the stop band. There still is a lack of quantitative understanding of the observed features. Experimental studies [9–15] so far have concentrated on the polarization of the emitted light, and theoretical work [9,11] in this field has focused on the polarization of emission at short wavelengths, far away from the stop band. The observed changes in emission intensity near the stop band have been qualitatively discussed by Voigt *et al.* [15], stressing the important role of the DOS for understanding the spectra. In this paper, we discuss the drastic changes in fluorescence intensity and polarization in the region of the stop band, and derive a quantitative theoretical description of the observed phenomena. We will show, that the observed changes in emission can be explained, if one takes into account the drastic changes in the DOS in this wavelength region. There is a close relation to the work of Tocci *et al.* [16], who studied spontaneous emission in a periodic 1D semiconductor heterostructure, and we will adopt to some

degree their approach [16,17] to calculate the DOS. However, we have to face some additional complications due to the optical anisotropy of the cholesteric medium and the anisotropic orientational distribution of the fluorescent guest molecules.

In an isotropic medium, the rate w of emission of a photon with certain polarization and certain wave vector $\boldsymbol{k}$ by an excited molecule is described by *Fermi's Golden Rule*, stating

$$w_{\mathrm{iso}} \sim \rho_{\mathrm{iso}} \left|\langle f|\boldsymbol{\mu}\cdot\boldsymbol{a}_k|i\rangle\right|^2, \tag{1}$$

where $\boldsymbol{\mu}$ is the dipole moment operator, $\boldsymbol{a}_k$ is the electromagnetic vector potential, i and f indicate the initial and final state, and ρ_{iso} is the DOS. In isotropic media, the DOS is independent of the polarization and the direction. The states i and f usually are not known in detail, so we characterize the molecular transition by a transition dipole moment $\boldsymbol{d}$, its coupling to the electric field $\boldsymbol{E}$ depending on the projection $\boldsymbol{E}^*\cdot\boldsymbol{d}$:

$$w_{\mathrm{iso}} \sim \rho_{\mathrm{iso}} |\boldsymbol{E}^*\cdot\boldsymbol{d}|^2. \tag{2}$$

On transition from the isotropic to the cholesteric phase, the medium becomes birefringent, and the emission depends on the orientation of the transition dipole moment $\boldsymbol{d}$ with respect to the cholesteric axis and the local director. In the following, we restrict our considerations on emission parallel to the cholesteric axis. The DOS now depends on the polarization. We assume that the excited molecule has to choose one of the two normal modes $\boldsymbol{E}_1$, $\boldsymbol{E}_2$ for emission, with respective emission probabilities

$$w_i \sim \rho_i |\boldsymbol{E}_i^*\cdot\boldsymbol{d}|^2, \tag{3}$$

where ρ_i is the DOS associated to the normal mode $\boldsymbol{E}_i$. The fluorescent molecules adopt to some degree the local nematic order of the cholesteric solvent, which results in an anisotropic orientational distribution of the transition dipole moment. We are interested in the change in emission of a CLC film with thickness D on transition from the isotropic to the cholesteric phase. Therefore we define the relative fluorescence intensities

$$\begin{aligned} I_i &= \frac{\int_0^D \langle w_i\rangle_{\mathrm{clc}}\mathrm{d}z}{\int_0^D \langle w_{\mathrm{iso}}\rangle_{\mathrm{iso}}\mathrm{d}z} \\ &= \frac{\rho_i}{\rho_{\mathrm{iso}}}\frac{\int_0^D \langle|\boldsymbol{E}_i^*\cdot\hat{\boldsymbol{d}}|^2\rangle_{\mathrm{clc}}\mathrm{d}z}{\int_0^D \langle|\boldsymbol{E}_{\mathrm{iso}}^*\cdot\hat{\boldsymbol{d}}|^2\rangle_{\mathrm{iso}}\mathrm{d}z}, \end{aligned} \tag{4}$$

where there brackets $\langle\ldots\rangle_{\mathrm{iso}}$ and $\langle\ldots\rangle_{\mathrm{clc}}$ denote the average over the orientational distribution of the transition dipole moment in the isotropic and the cholesteric phase, respectively. The normal mode $\boldsymbol{E}_{\mathrm{iso}}$ represents a plane wave with arbitrarily chosen polarization. The relative intensities I_i no longer depend on the absolute value of the transition dipole moment $\boldsymbol{d}$, only on its direction. Therefore, instead of $\boldsymbol{d}$ we use in equation (4) the unit vector $\hat{\boldsymbol{d}} = \boldsymbol{d}/|\boldsymbol{d}|$ (throughout this paper, unit vectors will be indicated by a caret ' ˆ '). In the following, we assume the fluorescent molecules to be homogeneously distributed in the film; then, the spatial dependence of the normal modes $\boldsymbol{E}_i$ no longer is important. The normal modes being normalized [17], we then get a simplified expression for the relative intensities:

$$I_i = \frac{\rho_i}{\rho_{\mathrm{iso}}}\frac{\langle|d_i|^2\rangle_{\mathrm{clc}}}{\langle|d_{\mathrm{iso}}|^2\rangle_{\mathrm{iso}}}, \tag{5}$$

with

$$d_i = \hat{\boldsymbol{e}}_i^*\cdot\hat{\boldsymbol{d}} \tag{6}$$

and

$$d_{\mathrm{iso}} = \hat{\boldsymbol{p}}^*\cdot\hat{\boldsymbol{d}}, \tag{7}$$

where $\hat{\boldsymbol{e}}_1$ and $\hat{\boldsymbol{e}}_2$ denote the polarizations of the two normal modes, and $\hat{\boldsymbol{p}}$ is an arbitrarily chosen polarization.

For the calculation of the DOS and the factors d_i, and as well for discussing the polarization of the emitted light, it will proof useful to use the results of de Vries' classical treatment of light propagation in CLCs, which provides exact results for the polarizations, dispersion relations, and reflection and transmission coefficients of the two normal modes for light propagation parallel to the cholesteric axis. In Section 2, we give a summary of the main results of the de Vries theory. In Section 3, we derive analytical expressions for the densities of states ρ_i of the two normal light modes propagating parallel to the cholesteric axis. In Section 4, we calculate the factors $\langle|d_i|^2\rangle$, and we discuss the change in emission intensity on transition from the isotropic to the cholesteric phase in terms of the DOS and an order parameter describing the degree of nematic alignment of the dye's transition dipole moment. In Section 5, we discuss the polarization of the emitted light. In Section 6, we shortly discuss the emission of a nematic film. In Section 7, we discuss limitations of our theory for small emission wavelengths. In Section 8, we give a description of our experimental setup and the investigated samples. Finally, in Section 9 we present our experimental results, which show excellent quantitative agreement with our theoretical predictions.

2 Main results of the de Vries theory

In this section, we summarize the main results of de Vries' theory of CLC optics. We consider light propagation parallel to the helical axis of a CLC with pitch p. The birefringence of the quasi-nematic planes is characterized by their refractive indices n_{o} and n_{e}. Right- and left-handed helical structures are represented by positive and negative values of p, respectively. It will proof useful to introduce the mean refractive index of the nematic planes,

$$\bar{n} = \sqrt{(n_{\mathrm{o}}^2 + n_{\mathrm{e}}^2)/2}, \tag{8}$$

the parameter

$$\alpha = \frac{n_{\mathrm{e}}^2 - n_{\mathrm{o}}^2}{2\bar{n}^2} \tag{9}$$

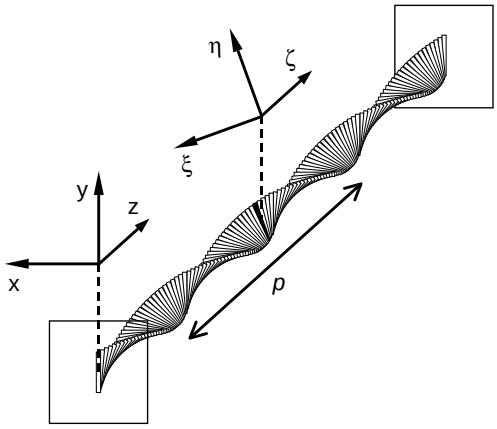

Fig. 1. Laboratory frame $\{\hat{\boldsymbol{x}}, \hat{\boldsymbol{y}}, \hat{\boldsymbol{z}}\}$ and rotating frame $\{\hat{\boldsymbol{\xi}}, \hat{\boldsymbol{\eta}}, \hat{\boldsymbol{\zeta}}\}$.

describing the relative dielectric anisotropy, and the reduced wavelength

$$\lambda' = \lambda/(\bar{n}p), \tag{10}$$

where λ is the wavelength in vacuo. Due to the sign convention introduced for p, negative and positive λ' values correspond to left- and right-handed helices, respectively. To describe the rotating director $\hat{\boldsymbol{n}}$, we start with a right-handed laboratory frame $\{\hat{\boldsymbol{x}}, \hat{\boldsymbol{y}}, \hat{\boldsymbol{z}}\}$, with $\hat{\boldsymbol{z}}$ parallel to the helical axis:

$$\hat{\boldsymbol{n}}(z) = -\sin(k_p z)\hat{\boldsymbol{x}} + \cos(k_p z)\hat{\boldsymbol{y}}, \tag{11}$$

with

$$k_p = 2\pi/p \tag{12}$$

being the wave number of the cholesteric twist. For light propagation parallel to the cholesteric axis, it is convenient to introduce a rotating coordinate system (Fig. 1) $\{\hat{\boldsymbol{\xi}}, \hat{\boldsymbol{\eta}}, \hat{\boldsymbol{\zeta}}\}$:

$$\begin{aligned} \hat{\boldsymbol{\xi}} &= \cos(k_p z)\hat{\boldsymbol{x}} + \sin(k_p z)\hat{\boldsymbol{y}}, \\ \hat{\boldsymbol{\eta}} &= -\sin(k_p z)\hat{\boldsymbol{x}} + \cos(k_p z)\hat{\boldsymbol{y}} = \hat{\boldsymbol{n}}, \\ \hat{\boldsymbol{\zeta}} &= \hat{\boldsymbol{z}}. \end{aligned} \tag{13}$$

In the rotating coordinate system, the two polarization eigenstates represent elliptically polarized waves $\boldsymbol{E}_1$, $\boldsymbol{E}_2$ with opposite handedness,

$$\boldsymbol{E}_{1,2} = \hat{\boldsymbol{e}}_{1,2} \exp(\mathrm{i}k_{1,2}\zeta) \tag{14}$$

(we consider propagation along the positive ζ-direction, and we omit the explicit time dependence $\exp(-\mathrm{i}\omega t)$). These basic waves have polarizations

$$\hat{\boldsymbol{e}}_i = \frac{1}{\sqrt{1+|f_i|^2}} \left(\hat{\boldsymbol{\xi}} + \mathrm{i}f_i\hat{\boldsymbol{\eta}}\right) \tag{15}$$

with ellipticities f_1, f_2. The wave numbers k_1, k_2 can be written in the form

$$k_i = 2\pi \frac{m_i'}{\lambda' p}\,. \tag{16}$$

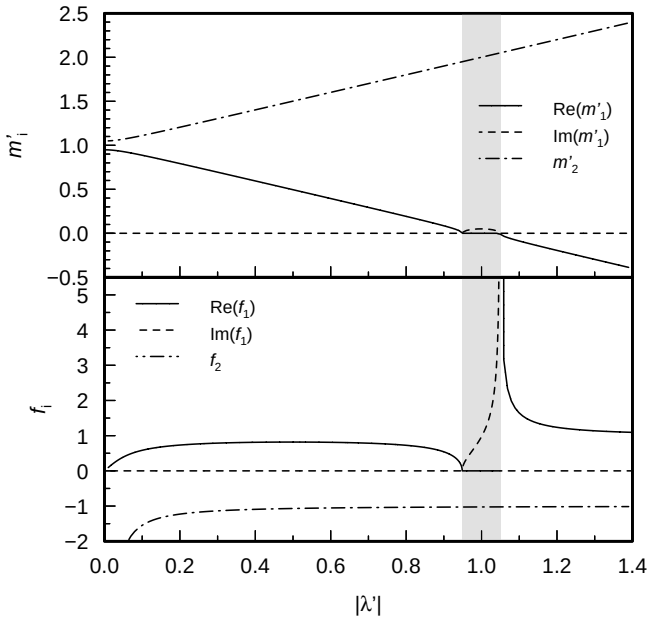

Fig. 2. 'Refractive indices' m_i' (top) and ellipticities f_i (bottom) for the basic waves $\boldsymbol{E}_1$, $\boldsymbol{E}_2$ in a CLC with anisotropy parameter $\alpha = 0.1$. The grey area marks the stop band.

The reduced 'refractive indices' $m_{1,2}'$ are roots of

$$m_{1,2}'^2 = 1 + \lambda'^2 \mp \sqrt{4\lambda'^2 + \alpha^2}. \tag{17}$$

For $|\lambda'| > \sqrt{1+\alpha}$, the *negative* root of $m_1'^2$ has to be used, resulting in a negative wave number k_1 (Eq. (16)) in the rotating coordinate system. m_1' and m_2' are plotted in Figure 2 as functions of the reduced wavelength, assuming $\alpha = 0.1$. For $\left|\lambda'^2 - 1\right| < \alpha$, $m_1'^2$ is negative and thus m_1' is imaginary, resulting in an imaginary wave number k_1: here, the wave $\boldsymbol{E}_1$ represents an evanescent wave. This wavelength region is the CLC's stop band. The ellipticities $f_{1,2}$ of the polarization eigenstates (Eq. (15)) read

$$f_i = \frac{1 - \alpha - m_i'^2 - \lambda'^2}{2m_i'\lambda'}\,. \tag{18}$$

They are also shown in Figure 2 (assuming a right-handed helix). Values $f_i = 0$ and $f_i = \pm\infty$ represent linear polarized waves with the electric field parallel to the $\hat{\boldsymbol{\xi}}$ and $\hat{\boldsymbol{\eta}}$ direction, respectively. For wavelengths $|\lambda'| \ll \alpha$, the two basic waves are nearly linearly polarized. For $|\lambda'| \gg \alpha$, $\boldsymbol{E}_2$ shows almost perfect circular polarization. This also holds for the wave $\boldsymbol{E}_1$ far away from the stop band. However, in the vicinity of the stop band its polarization changes drastically, and at the band edges it forms a linearly polarized wave – at the long-wavelength edge parallel to the local director ($\hat{\boldsymbol{\eta}}$ direction), at the short-wavelength perpendicular to the local director. Inside the stop band, f_1 is imaginary, resulting in a linear polarization $\hat{\boldsymbol{e}}_1$ of the evanescent wave $\boldsymbol{E}_1$. One should note a bizarre feature of the two eigenpolarizations $\hat{\boldsymbol{e}}_1$, $\hat{\boldsymbol{e}}_2$: in general, they are *not* orthogonal ($\hat{\boldsymbol{e}}_1^* \cdot \hat{\boldsymbol{e}}_2 \neq 0$) [1].

For the calculation of the DOS and of the polarization of the fluorescence light outside the film, we will need the reflection and transmission properties of the glass-CLC and CLC-glass interfaces. De Vries assumed the surrounding medium to have the refractive index $\bar{n}$ (Eq. (8)). This index matching is a good approximation for most cholesterics sandwiched between glass slides. It is useful to introduce the quantity

$$q_i = \lambda' f_i + m_i'. \tag{19}$$

The incident wave $\boldsymbol{E}_i^{\mathrm{in}}$ resulting inside the CLC in the wave $\exp(\mathrm{i}k_i\zeta)\hat{\boldsymbol{e}}_i$ is an elliptically polarized wave,

$$\boldsymbol{E}_i^{\mathrm{in}}(z=0) = \left[\frac{1+(f_i/q_i)^2}{1+|f_i|^2}\right]^{1/2} \frac{1+q_i}{2}\hat{\boldsymbol{e}}_i^{\mathrm{iso}}, \tag{20}$$

with

$$\hat{\boldsymbol{e}}_i^{\mathrm{iso}} = \frac{1}{\sqrt{1+(f_i/q_i)^2}}\left(\hat{\boldsymbol{x}} + \mathrm{i}\frac{f_i}{q_i}\hat{\boldsymbol{y}}\right). \tag{21}$$

At the CLC-glass interface, each normal mode gives rise to a reflected wave which also only consists of the respective basic wave [2]; the reflection coefficient r_i for the wave $\boldsymbol{E}_i$ reads

$$r_i = -\frac{1-q_i}{1+q_i}\cdot \tag{22}$$

In the surrounding medium, the basic wave $\boldsymbol{E}_i$ results in an elliptically polarized outgoing wave $\boldsymbol{E}_i^{\mathrm{out}}$. Assuming unit intensity of the basic wave at the CLC-glass interface, the amplitude of the transmitted wave reads

$$\boldsymbol{E}_i^{\mathrm{out}} = \left[\frac{1+(f_i/q_i)^2}{1+|f_i|^2}\right]^{1/2} \frac{2q_i}{1+q_i}\hat{\boldsymbol{e}}_i^{\mathrm{iso}} \tag{23}$$

(again we assume a matching of the coordinate systems $\{\hat{\boldsymbol{\xi}}, \hat{\boldsymbol{\eta}}, \hat{\boldsymbol{\zeta}}\}$ and $\{\hat{\boldsymbol{x}}, \hat{\boldsymbol{y}}, \hat{\boldsymbol{z}}\}$ at the interface). For $|\lambda'| \gg \alpha$, the waves $\boldsymbol{E}_i^{\mathrm{in}}$ and $\boldsymbol{E}_i^{\mathrm{out}}$ are almost circularly polarized. The two polarizations $\hat{\boldsymbol{e}}_1^{\mathrm{iso}}$, $\hat{\boldsymbol{e}}_2^{\mathrm{iso}}$ are orthogonal ($(\hat{\boldsymbol{e}}_1^{\mathrm{iso}})^* \cdot \hat{\boldsymbol{e}}_2^{\mathrm{iso}} = 0$).

3 Photonic density of states in a cholesteric film

The photonic density of states (DOS) ρ may be defined as the inverse slope of the dispersion relation,

$$\rho = \left|\frac{\mathrm{d}}{\mathrm{d}\omega}\mathrm{Re}(k)\right|, \tag{24}$$

thus counting the number of light modes per unit frequency ω (the DOS being a real quantity, only the real part of k is relevant). We consider light propagation in a CLC film parallel to the helical axis. We use reduced wave numbers

$$k_i' = k_i p. \tag{25}$$

In an isotropic medium with refractive index $\bar{n}$, the DOS is

$$\rho_{\mathrm{iso}} = \bar{n}/c, \tag{26}$$

where c is the speed of light in vacuo. For a birefringent medium like a CLC, we introduce two densities of states, ρ_1, ρ_2, one for each polarization eigenstate separately. First we consider the DOS $\rho_i^{(\infty)}$ in a thick cholesteric slab, where effects due to multiple reflections at the interfaces can be neglected. Then for the calculation of the DOS we have to use the dispersion of the two basic waves $\boldsymbol{E}_1$, $\boldsymbol{E}_2$ (Eq. (14)). It should be noted, that there is no need to transform the waves $\boldsymbol{E}_1$, $\boldsymbol{E}_2$ (which describe light propagation in the rotating coordinate system $\{\hat{\boldsymbol{\xi}}, \hat{\boldsymbol{\eta}}, \hat{\boldsymbol{\zeta}}\}$) back to the laboratory system $\{\hat{\boldsymbol{x}}, \hat{\boldsymbol{y}}, \hat{\boldsymbol{z}}\}$: this operation changes the wave number $k_{1,2}$ (Eq. (16)) in the $\{\hat{\boldsymbol{\xi}}, \hat{\boldsymbol{\eta}}, \hat{\boldsymbol{\zeta}}\}$-system just by the constant wave number k_p of the cholesteric twist (Eq. (12)), which is cancelled again when taking the derivative according to equation (24). In the stop band, the wave number k_1 of $\boldsymbol{E}_1$ is imaginary. Thus its DOS is exactly zero. Now we consider the case of real wave numbers k_i. According to equation (16), k_i is given as a function of the reduced wavelength λ', explicitly by the factor $1/\lambda'$, and implicitly by the λ'-dependent factor m_i'. Thus we calculate the DOS $\rho_i^{(\infty)}$ as follows:

$$\rho_i^{(\infty)} = p^{-1}\frac{\mathrm{d}k_i'}{\mathrm{d}\lambda'}\frac{\mathrm{d}\lambda'}{\mathrm{d}\omega}\cdot \tag{27}$$

The derivatives occurring on the right hand side of equation (27) are listed in the Appendix (Eqs. (A.1) and (A.3)), as well as all other derivatives of basic optical quantities needed for our further calculations.

In thin cholesteric films, multiple reflections at the interfaces result in a superposition of waves traveling in the $+\hat{\boldsymbol{\zeta}}$ and $-\hat{\boldsymbol{\zeta}}$ direction. We consider a film of thickness Np (N revolutions of the director), with the interfaces located in the $\{\hat{\boldsymbol{\xi}}$-$\hat{\boldsymbol{\eta}}\}$-planes at $\zeta = 0$ and $\zeta = N|p|$. We use a reduced $\hat{\boldsymbol{\zeta}}$-coordinate $z' = \zeta/|p|$. To calculate the DOS, we proceed in a way similar to that of Bendickson *et al.* [17]: it is convenient to define an effective wave number $k'_{\mathrm{eff},i}$ by identifying the product $k'_{\mathrm{eff},i}N$ with the phase difference of the total field amplitude at the two interfaces of the film. With the help of the complex amplitude transmission coefficient

$$T_i = X_i + \mathrm{i}Y_i \tag{28}$$

for propagation of the basic wave $\boldsymbol{E}_i$ through the CLC film, we then can formulate the dispersion relation

$$\tan\left(k'_{\mathrm{eff},i}N\right) = \frac{Y_i}{X_i}\cdot \tag{29}$$

Taking on both sides the derivative with respect to ω,

$$\sec^2(k'_{\mathrm{eff},i}N)\frac{\mathrm{d}k'_{\mathrm{eff},i}}{\mathrm{d}\omega} = \frac{1}{N}\frac{X_i(\mathrm{d}Y_i/\mathrm{d}\omega) - Y_i(\mathrm{d}X_i/\mathrm{d}\omega)}{X_i^2} \tag{30}$$

and using the identity

$$\sec^2(k'_{\mathrm{eff},i}N) = \tan^2(k'_{\mathrm{eff},i}N) + 1 = Y_i^2/X_i^2 + 1, \quad (31)$$

one finally obtains the DOS

$$\rho_i = p^{-1}\frac{\mathrm{d}k'_{\mathrm{eff},i}}{\mathrm{d}\omega} = \frac{1}{Np}\frac{X_i(\mathrm{d}Y_i/\mathrm{d}\omega) - Y_i(\mathrm{d}X_i/\mathrm{d}\omega)}{X_i^2 + Y_i^2} \quad (32)$$

in terms of the real and imaginary part of the transmission coefficient T_i. To obtain the transmission coefficient of the film, we have to calculate the total complex field amplitude at the rear ($z' = N$) of the film. We start with a wave $\boldsymbol{E}_i^{\mathrm{in}}$ traveling in $+\hat{\boldsymbol{\zeta}}$ direction, which results on passing the $z' = 0$ - interface in the basic wave $\boldsymbol{E}_i$. The passage of the interface changes the field amplitude according to equation (20). Important for the calculation of the DOS is only the phase jump of the wave on traversing the interface, not the change in intensity. Except for $\boldsymbol{E}_1$ inside the stop band, both the incident and transmitted wave are elliptically polarized waves, and the phase jump is zero (the prefactor $(1 + q_i)/2$ in Eq. (20) being real). For $\boldsymbol{E}_1$ at wavelengths inside the stop band, the incoming elliptically polarized wave generates an evanescent wave. There is no unique rule to define a phase relation between these two waves at the interface. To the incident wave at the location of the interface, and to the evanescent mode we assign the phases $\phi_1^{\mathrm{in}} = \arg(1+q_1)$ (as suggested by the prefactor appearing in Eq. (20)) and $\phi_1 = 0$, respectively. Thus, the phase jump on traversing the interface is

$$\Delta\phi_1 = \arg(1 + q_1^*) = \arg(1 - q_1). \quad (33)$$

Other definitions of the phases ϕ_1^{in} and ϕ_1 would result in an additive wavelength-independent term for the phase jump, which has no effect on the calculation of the DOS. Therefore, as transmission coefficient of the incident wave at the $z' = 0$-interface we use

$$t_i = 1 - q_i. \quad (34)$$

On traversing the film once, the wave accumulates a phase factor $\exp(\mathrm{i}Nk'_i)$. On reflection at the CLC-glass interface, the wave is altered by the reflection coefficient r_i (Eq. (22)). The sum of all the resulting back- and forthreflected waves results in a geometric series for the amplitude at the $z' = N$-interface. The series can be reduced to

$$T_i = t_i(1 + r_i)\frac{\exp(\mathrm{i}k'_iN)}{1 - r_i^2\exp(\mathrm{i}2k'_iN)}\,. \quad (35)$$

To calculate the DOS according to equation (32), the transmission coefficient T_i has to be split in its real (X_i) and imaginary (Y_i) part. It should be noted, that common real prefactors of X_i and Y_i cancel themselves in the calculation of the DOS, and therefore may be omitted. The transmission coefficient T_i is a function of the parameters t_i, r_i, and k'_i, which themselves are given in the framework of the de Vries theory as functions of the reduced wavelength λ'. Thus the derivatives of X_i and Y_i appearing in the DOS (Eq. (32)) are conveniently written in the form

$$\frac{\mathrm{d}X_i}{\mathrm{d}\omega} = \frac{\mathrm{d}X_i}{\mathrm{d}\lambda'}\frac{\mathrm{d}\lambda'}{\mathrm{d}\omega} \quad \text{and} \quad \frac{\mathrm{d}Y_i}{\mathrm{d}\omega} = \frac{\mathrm{d}Y_i}{\mathrm{d}\lambda'}\frac{\mathrm{d}\lambda'}{\mathrm{d}\omega}\,. \quad (36)$$

For splitting T_i in its real and imaginary part, we have to consider two cases: (1) for the basic wave $\boldsymbol{E}_1$ outside the stop band, and for the basic wave $\boldsymbol{E}_2$ at all wavelengths, t_i, r_i and k_i are real; (2) inside the stop band, t_1 and r_1 are complex and k_1 is imaginary. In case (1), multiplication of the right hand side of equation (35) with the complex conjugate of the denominator, and omitting the irrelevant common real prefactors, yields

$$X_i = \left(1 - r_i^2\right)\cos(k'_iN), \quad (37)$$

$$Y_i = \left(1 + r_i^2\right)\sin(k'_iN). \quad (38)$$

The derivatives with respect to λ' read

$$\frac{\mathrm{d}X_i}{\mathrm{d}\lambda'} = -2r_i\cos(k'_iN)\frac{\mathrm{d}r_i}{\mathrm{d}\lambda'} - (1 - r_i^2)N\sin(k'_iN)\frac{\mathrm{d}k'_i}{\mathrm{d}\lambda'}, \quad (39)$$

$$\frac{\mathrm{d}Y_i}{\mathrm{d}\lambda'} = 2r_i\sin(k'_iN)\frac{\mathrm{d}r_i}{\mathrm{d}\lambda'} + (1 + r_i^2)N\cos(k'_iN)\frac{\mathrm{d}k'_i}{\mathrm{d}\lambda'}\,. \quad (40)$$

The derivatives $\mathrm{d}k'_i/\mathrm{d}\lambda'$ and $\mathrm{d}r_i/\mathrm{d}\lambda'$ are given in the Appendix (Eqs. (A.3) and (A.8)). In case (2), we write the complex parameters in the form $k'_1 = \mathrm{i}\tilde{k}'_1$, $r_1 = r_\mathrm{a} + \mathrm{i}r_\mathrm{b}$ (r_a, r_b real) and $t_1 = 1 - \mathrm{i}\tilde{q}_1$. Again omitting common real prefactors, we obtain

$$X_1 = AC - BD \qquad \text{and} \qquad Y_1 = AD + BC, \quad (41)$$

with

$$A = 1 + r_\mathrm{a} + \tilde{q}_1 r_\mathrm{b}, \quad (42)$$

$$B = r_\mathrm{b} - \tilde{q}_1(1 + r_\mathrm{a}), \quad (43)$$

$$C = 1 - \left(r_\mathrm{a}^2 - r_\mathrm{b}^2\right)\exp\left(-2\tilde{k}'_1N\right), \quad (44)$$

$$D = 2r_\mathrm{a}r_\mathrm{b}\exp\left(-2\tilde{k}'_1N\right). \quad (45)$$

The derivatives needed for the calculation of the DOS according to equation (36) now read

$$\frac{\mathrm{d}X_1}{\mathrm{d}\lambda'} = \frac{\mathrm{d}A}{\mathrm{d}\lambda'}C + A\frac{\mathrm{d}C}{\mathrm{d}\lambda'} - \frac{\mathrm{d}B}{\mathrm{d}\lambda'}D - B\frac{\mathrm{d}D}{\mathrm{d}\lambda'} \quad (46)$$

(and similarly for $\mathrm{d}Y_1/\mathrm{d}\lambda'$). The derivatives of A, B, C, D with respect to λ' are listed in the Appendix, equations (A.16–A.19).

In the top of Figure 3, we show the relative DOS $\rho_1/\rho_{\mathrm{iso}}$ of the wave with polarization $\hat{\boldsymbol{e}}_1$, calculated for relative dielectric anisotropy $\alpha = 0.1$, and three different film thicknesses $N|p|$, as indicated in the figure; also plotted is the relative DOS $\rho_1^{(\infty)}/\rho_{\mathrm{iso}}$ of a thick film, calculated according to equation (27). The DOS of the thick

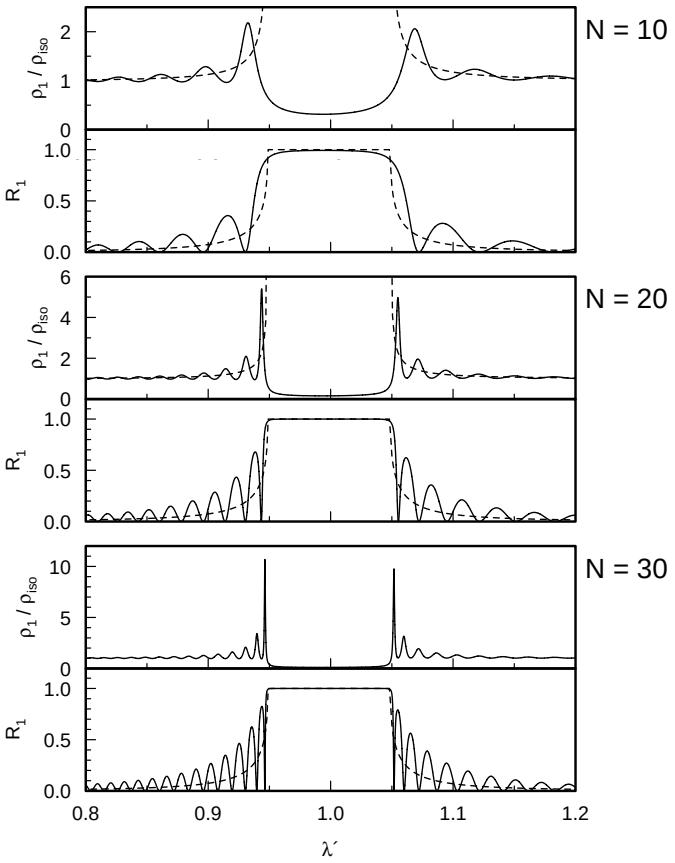

Fig. 3. Relative DOS $\rho_1/\rho_{\rm iso}$ and reflectivity R_1 of the wave with polarization $\hat{\boldsymbol{e}}_1$, using $\alpha = 0.1$. Solid curves calculated for the film thicknesses $N|p|$ indicated on the right; dashed curves calculated for infinite thickness (*i.e.*, neglecting multiple reflections).

film diverges at the band edges, and inside the stop band, it is exactly zero. In case of a thin film, the DOS shows Fabry-Perot-like oscillations, growing in amplitude on approaching the stop band. In contrast to $\rho_1^{(\infty)}/\rho_{\rm iso}$, it remains finite inside the stop band, because the superposition of the multiple-'reflected' evanescent waves no longer is completely evanescent, but contains a propagating component. As to be expected, on increasing the film thickness the resonance peaks become more and more pronounced and closely spaced. The relative DOS $\rho_2/\rho_{\rm iso}$ (not plotted in Fig. 3) is very close to unity, showing only tiny oscillations. Also shown in Figure 3 are the reflectivity curves for light with polarization $\hat{\boldsymbol{e}}_1$, calculated with the same parameters α, N as used for the relative DOS. The Fabry-Perot fringes are oscillating around the reflectivity curve of the thick film (dashed line), in a similar fashion as the oscillations found for the DOS. The maxima of the reflectivity almost coincide with minima of the DOS (this matching improves on increasing the film thickness).

4 Intensity of the emitted light

After calculating the DOS of the two normal modes, the second step in the calculation of the relative intensities

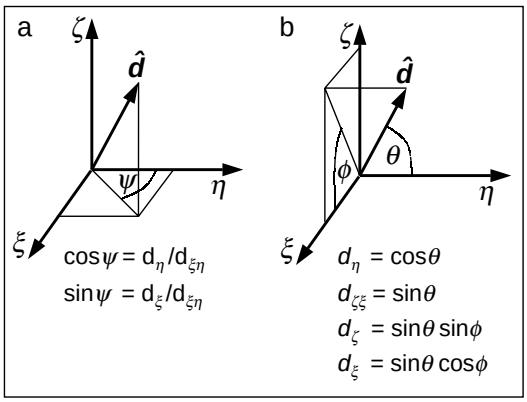

Fig. 4. Angles used to describe the orientation of the transition dipole moment $\hat{\boldsymbol{d}}$.

I_i (Eq. (5)) is the determination of the average $\langle |d_i|^2 \rangle$ of the squared projections of the transition dipole moment $\hat{\boldsymbol{d}}$ on the polarization eigenstates $\hat{\boldsymbol{e}}_i$. For the calculation of the factors d_i, only the projection $\boldsymbol{d}_{\xi\eta}$ on the $\{\hat{\boldsymbol{\xi}}, \hat{\boldsymbol{\eta}}\}$ – plane is relevant. We characterize its orientation by the angle ψ with respect to the local director, *i.e.* the $\hat{\boldsymbol{\eta}}$ – axis (Fig. 4a):

$$\boldsymbol{d}_{\xi\eta} = d_{\xi\eta}(\sin\psi\,\hat{\boldsymbol{\xi}} + \cos\psi\,\hat{\boldsymbol{\eta}}). \tag{47}$$

Using the expressions for the polarization eigenstates (Eq. (15)), the factors $|d_i|^2$ then read in general

$$|d_i|^2 = d_{\xi\eta}^2 \frac{1 + (f_i^2 - 1)\cos^2\psi}{1 + f_i^2}, \tag{48}$$

except for d_1 at wavelengths inside the stop band; here, $\hat{\boldsymbol{E}}_1$ is linearly polarized, due to the imaginary ellipticity f_1. Writing $f_1 = \mathrm{i}\tilde{f}_1$, we get

$$|d_1|^2 = d_{\xi\eta}^2 \frac{1 + \left(\tilde{f}_1^2 - 1\right)\cos^2\psi}{1 + \tilde{f}_1^2} - \frac{2\tilde{f}_1}{1 + \tilde{f}_1^2}\, d_{\xi\eta}^2 \sin\psi\cos\psi. \tag{49}$$

To obtain the change in emission of the dye-doped cholesteric film, the factors $|d_i|^2$ have to be averaged according to the orientational distribution of the transition dipole moment. In analogy to the order parameter S used to quantify the molecular orientational order in nematic liquid crystals [1], we characterize the degree of order of the transition dipole moment by an order parameter $S_{\rm d}$. It is defined as the average

$$S_{\rm d} = \frac{3}{2}\left\langle \cos^2\theta \right\rangle - \frac{1}{2}, \tag{50}$$

where θ is the angle between the local director ($\hat{\boldsymbol{\eta}}$ – direction) and the transition dipole moment (Fig. 4b). The maximum possible value $S_{\rm d} = 1$ corresponds to the (hypothetical) case of perfect alignment of the transmission

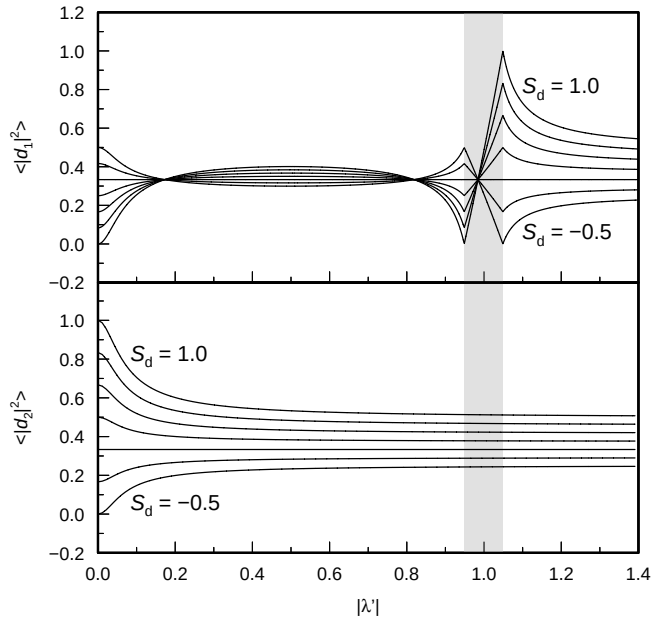

Fig. 5. The averages $\langle |d_i|^2 \rangle$ as a function of the reduced wavelength, for $\alpha = 0.1$; curves are calculated using S_d – values ranging from -0.5 to 1 in steps of 0.25. Curves corresponding to $S_\mathrm{d} = -0.5$ and $S_\mathrm{d} = 1$ are marked accordingly. The grey area marks the stop band.

dipole moment parallel to the local director $\hat{\boldsymbol{n}}$. $S_\mathrm{d} = 0$ corresponds to an isotropic orientational distribution. Values $S_\mathrm{d} < 0$ correspond to a preferred orientation perpendicular to $\hat{\boldsymbol{n}}$ (the minimum value $S_\mathrm{d} = -0.5$ corresponding to an isotropic distribution restricted on the plane perpendicular to $\hat{\boldsymbol{n}}$). To determine the averaged factor $\langle d_i \rangle$ in terms of the order parameter S_d, we start with an arbitrarily oriented dipole moment $\hat{\boldsymbol{d}}$, characterized by angles θ and ϕ as indicated in Figure 4b. The projection of the transition dipole moment on the $\{\hat{\boldsymbol{\xi}}, \hat{\boldsymbol{\eta}}\}$-plane then is

$$\begin{aligned} d_{\xi\eta} &= \left(d_\xi^2 + d_\eta^2\right)^{1/2} = \left[\left(1 - \cos^2\theta\right)\cos^2\phi + \cos^2\theta\right]^{1/2} \\ &= \left(\cos^2\theta\,\sin^2\phi + \cos^2\phi\right)^{1/2}. \end{aligned} \tag{51}$$

Using the identity

$$\cos\psi = \cos\theta / d_{\xi\eta}, \tag{52}$$

we now can perform the orientational average of the factors $|d_i|^2$. We first consider the case of real f_i (Eq. (48)),

$$\left\langle |d_i|^2 \right\rangle = \frac{1}{1+f_i^2} \left\langle \left\langle d_{\xi\eta}^2 \left[1 + (f_i^2 - 1)\cos^2\psi\right] \right\rangle_\phi \right\rangle_\theta, \tag{53}$$

where the brackets $\langle \ldots \rangle_\phi$, $\langle \ldots \rangle_\theta$ indicate the average over ϕ and θ, respectively. To perform the average, we insert equations (51) and (52), and use $\langle \cos^2\phi \rangle_\phi = \langle \sin^2\phi \rangle_\phi = \frac{1}{2}$ (the orientational distribution is assumed to have rotational symmetry along the director). We obtain

$$\left\langle |d_i|^2 \right\rangle = \frac{1}{1+f_i^2} \left[\left(f_i^2 - \frac{1}{2} \right) \langle \cos^2\theta \rangle_\theta + \frac{1}{2} \right]. \tag{54}$$

Employing the definition of the order parameter S_d (Eq. (50)), we finally get the result

$$\left\langle |d_i|^2 \right\rangle = \frac{2}{3} \frac{f_i^2 - \frac{1}{2}}{f_i^2 + 1} S_\mathrm{d} + \frac{1}{3}. \tag{55}$$

Substituting f_1 with $\tilde{f}_1$, this also holds for d_1 at wavelengths inside the stop band, because the additional term occurring in equation (49) vanishes when performing the average: it is proportional to $d_{\xi\eta}^2 \sin\psi\cos\psi$, and

$$\begin{aligned} \langle d_{\xi\eta}^2 \sin\psi\cos\psi \rangle &= \langle d_\eta d_\xi \rangle \\ &= \langle \langle \cos\theta \sin\theta \cos\phi \rangle_\phi \rangle_\theta \\ &= 0. \end{aligned} \tag{56}$$

Here we used the trigonometric relations listed in Figure 4 and the relation $\langle \cos\phi \rangle_\phi = 0$ (due to the rotational symmetry of the orientational distribution). Assuming $S_\mathrm{d} = 0$ (isotropic orientational distribution), equation (55) gives the average

$$\left\langle \left| d_\mathrm{iso}^2 \right| \right\rangle_\mathrm{iso} = \frac{1}{3} \tag{57}$$

needed for the calculation of the relative intensities according to equation (5). In Figure 5, the averages $\langle |d_i|^2 \rangle$ are plotted for several values of the order parameter S_d. The factor $\langle |d_2|^2 \rangle$ is a very smooth function of λ'. For not too small wavelengths it is almost constant, due to the almost constant polarization $\hat{\boldsymbol{e}}_2$. Higher values of S_d result in higher values of the factor $\langle |d_2|^2 \rangle$, because then the orientational distribution of the transition dipole moment is more and more concentrated along the local director, and thus its projection $\boldsymbol{d}_{\xi\eta}$ on the plane of the almost circular polarization $\hat{\boldsymbol{e}}_2$ is on the average higher. Near the stop band, there is a strong variation in $\langle |d_1|^2 \rangle$, due to the strong changes in the polarization $\hat{\boldsymbol{e}}_1$. Near the long-wavelength band edge, there is a major polarization component along the local director (diverging ellipticity f_1), resulting in high $\langle |d_1|^2 \rangle$-values for high order parameters S_d. Near the short-wavelength edge, $\hat{\boldsymbol{e}}_1$ is essentially perpendicular to the local director ($f_1 \approx 0$), thus a high order parameter S_d results in a low value of $\langle |d_1|^2 \rangle$.

Now we have all ingredients to calculate the relative fluorescence intensities I_1 and I_2 (Eq. (5)) as a function of the reduced emission wavelength in terms of the relative dielectric anisotropy α, the film thickness and the order parameter S_d of the dye's transition dipole moment.

In Figure 6, the relative intensities of a thick cholesteric slab (neglecting multiple reflections) are plotted for several values of the order parameter S_d, using $\alpha = 0.1$. Inside the stop band, I_1 vanishes, because $\rho_1 = 0$. If for S_d the extremal value -0.5 is chosen, I_1 diverges at the short-wavelength edge of the stop band, while at the other edge it remains a continuous function: there, the transition dipole moment is oriented completely in the plane perpendicular to the local director, so it can't emit into the resonant mode (whose polarization $\hat{\boldsymbol{e}}_1$ is parallel to the local director). Increasing the order parameter S_d, the divergence at the short-wavelength edge of the stop band

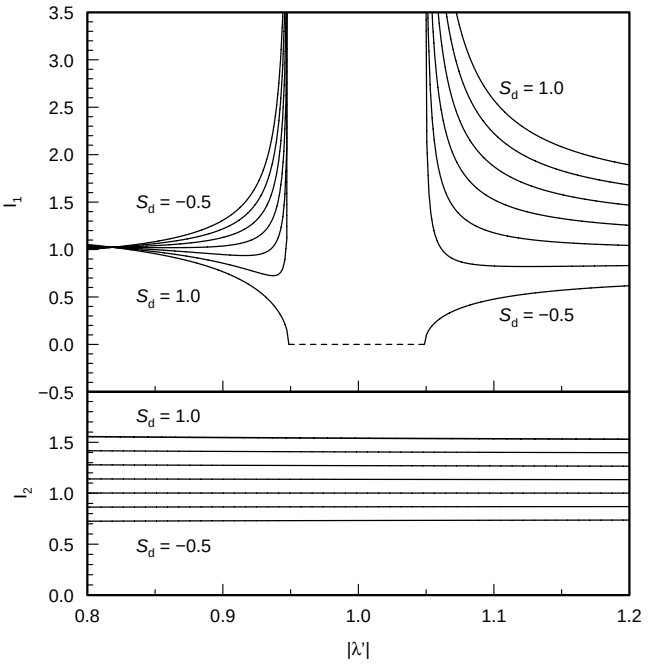

Fig. 6. Relative intensity contributions I_1 (top) and I_2 (bottom) of a thick cholesteric slab (neglecting multiple reflections), for $\alpha = 0.1$; curves are calculated using S_d – values ranging from -0.5 to 1 in steps of 0.25. Curves corresponding to $S_\mathrm{d} = -0.5$ and $S_\mathrm{d} = 1$ are marked accordingly. Inside the stop band, $I_1 = 0$ for all values of S_d (dashed line).

gets less pronounced, and at the long-wavelength edge, a second divergence emerges. For $S_\mathrm{d} = 1$, *i.e.* perfect alignment of the transition dipole moment along the local director, the short-wavelength divergence vanishes, because at this wavelength now the polarization of the resonant mode is oriented perpendicular to the transition dipole moments. For a given order parameter S_d, ρ_2, as well as $\langle|d_2|^2\rangle$, are almost constant, resulting in an almost constant intensity I_2.

Now we consider thin films, taking into account multiple reflections. In Figure 7, the relative intensity I_1 is plotted for various film thicknesses and order parameters S_d. Instead of the two divergences found for the thick CLC slab, now there are two dominant intensity peaks near the band edges. Changing the order parameter, their relative weight changes in a similar fashion as found for the divergences in case of the thick CLC slab: on increasing S_d, the long-wavelength resonance becomes more and more dominant. Increasing the film thickness N results in improved resonator quality of the film and thus in sharper intensity peaks.

5 Polarization of the emitted light

Widely used to characterize the polarization of the fluorescence light is the dissymmetry factor g_e,

$$g_\mathrm{e} = 2\frac{I_\mathrm{L} - I_\mathrm{R}}{I_\mathrm{L} + I_\mathrm{R}}, \tag{58}$$

where I_L and I_R denote the left- and righthanded circularly polarized intensity contributions. Possible values of g_e range from -2 to $+2$. To calculate the dissymmetry factor, we have to take into account that on passing the interface, the waves $\boldsymbol{E}_1$, $\boldsymbol{E}_2$ change their polarizations. Outside the film they have polarizations $\hat{\boldsymbol{e}}_i^\mathrm{iso}$ (Eq. (21)). For not too small wavelengths ($\lambda' > \alpha$), these are almost circular polarizations, so it is a good approximation to use the intensities I_1, I_2 instead of I_L, I_R for the calculation of the dissymmetry factor g_e. For an exact calculation of the dissymmetry factor, we decompose the two intensity contributions I_1, I_2 (Eq. (5)) in their respective right- and lefthanded CP components by calculating the scalar products of their respective field amplitudes

$$\boldsymbol{E}_i^\mathrm{out} = \hat{\boldsymbol{e}}_i^\mathrm{iso}\sqrt{I_i} \tag{59}$$

and the complex polarization vectors

$$\hat{\boldsymbol{e}}_+ = \frac{1}{\sqrt{2}}(\hat{\boldsymbol{x}} + \mathrm{i}\hat{\boldsymbol{y}}) \qquad \text{and} \qquad \hat{\boldsymbol{e}}_- = \frac{1}{\sqrt{2}}(\hat{\boldsymbol{x}} - \mathrm{i}\hat{\boldsymbol{y}}) \tag{60}$$

characterizing the two circular polarizations with opposite sense of rotation. For the amplitudes E_i^+, E_i^- of the two circularly polarized components we obtain

$$E_i^\pm = \frac{q_i \pm f_i}{\sqrt{|q_i|^2 + |f_i|^2}}\sqrt{I_i/2}. \tag{61}$$

Thus the two components have intensities

$$I_i^\pm = \frac{1}{2}\frac{|q_i \pm f_i|^2}{|q_i|^2 + |f_i|^2} I_i. \tag{62}$$

Using the sums $I_\mathrm{L} = I_1^+ + I_2^+$ and $I_\mathrm{R} = I_1^- + I_2^-$, we can now calculate the dissymmetry factor g_e according to equation (58). In Figure 8, the result for a thick cholesteric slab (neglecting multiple reflections) is plotted for various order parameters S_d, using $\alpha = 0.1$. We assume a lefthanded CLC (g_e changes its sign for a helix with opposite handedness). Except for the extreme values $S_\mathrm{d} = -0.5$ and $S_\mathrm{d} = 1$, there are discontinuities at both band edges: the polarization shows an abrupt reversal of its sense of rotation. Inside the stop band, the curves coincide (indicated by the dashed line), because in this wavelength region emission is restricted on waves with polarization $\hat{\boldsymbol{e}}_2$; here, the emission is almost completely circularly polarized (for $\alpha = 0.1$, $g_\mathrm{e} \approx -1.9975$). Outside the stop band, g_e approaches (almost) 2, because here emission is dominated by the mode with polarization $\hat{\boldsymbol{e}}_1$. In Figure 9, the dissymmetry factor is plotted for various film thicknesses and order parameters S_d. The discontinuities found for the thick CLC slab are no longer present, and oscillations occur due to the oscillations of the intensity contribution I_1. Increasing the film thickness, the dissymmetry factor more and more approaches its extremal value -2 inside the stop band, because emission gets more and more restricted on the mode with polarization $\hat{\boldsymbol{e}}_2$.

6 Emission of a nematic film

In the experimental section, we will present a supplementary measurement with a dye-doped nematic film. In the

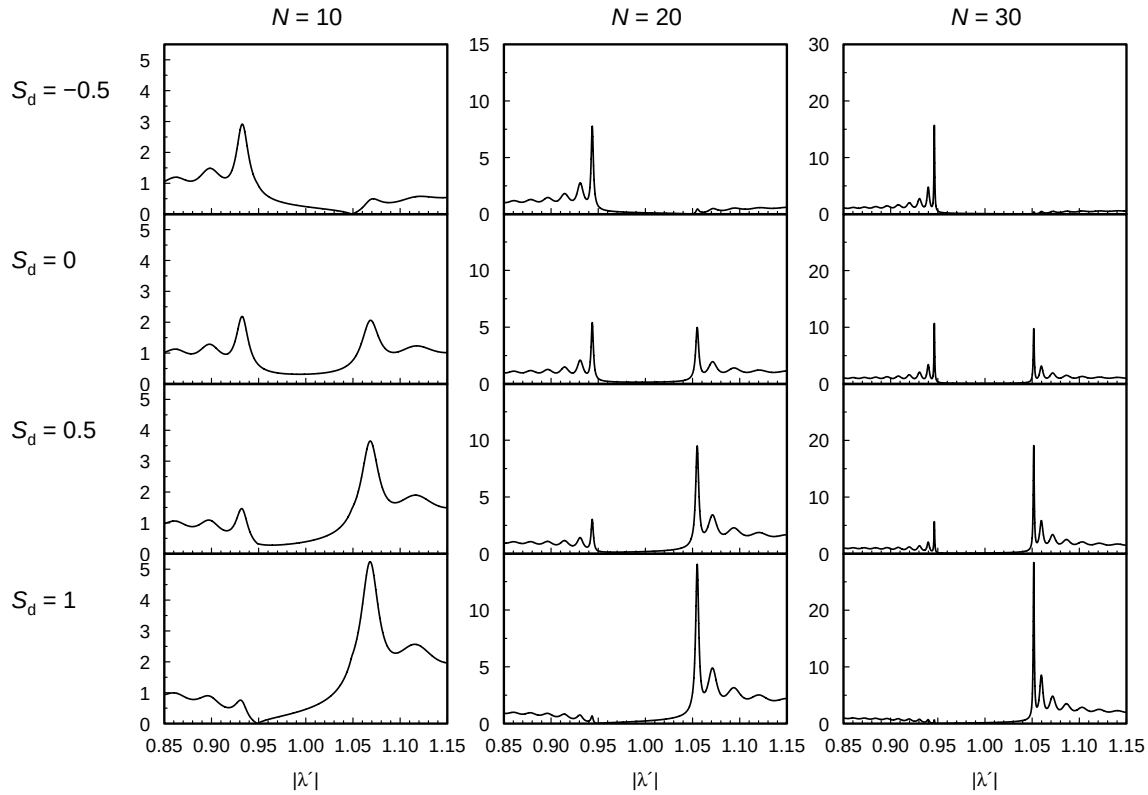

Fig. 7. Relative intensity contribution I_1 (taking into account multiple reflections), for $\alpha = 0.1$. The three columns correspond to the film thicknesses $N|p|$ as indicated at the top, the four rows correspond to the order parameters S_d indicated on the left.

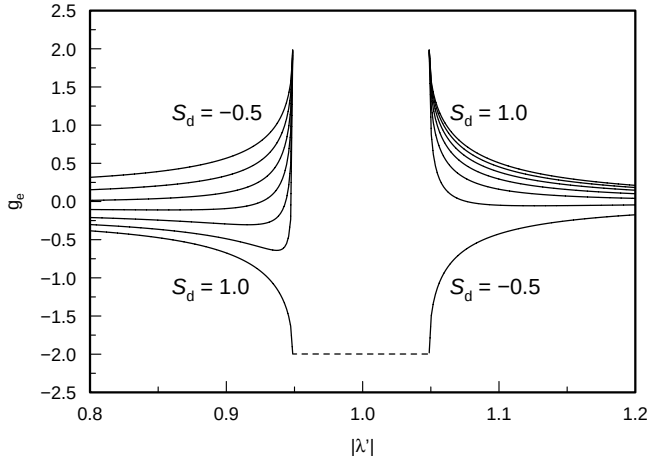

Fig. 8. Dissymmetry factor g_e for the fluorescence of a thick CLC slab (neglecting multiple reflections), assuming $\alpha = 0.1$ and a lefthanded cholesteric helix; curves are calculated using S_d-values ranging from -0.5 to 1 in steps of 0.25. Curves corresponding to $S_\mathrm{d} = -0.5$ and $S_\mathrm{d} = 1$ are marked accordingly. Inside the stop band, all curves coincide (dashed line).

following, we will briefly discuss how to derive the order parameter S_d from the ratio

$$r = I_\parallel / I_\perp \tag{63}$$

of the emission contributions $I_\parallel$, $I_\perp$ polarized parallel and perpendicular to the nematic director $\hat{\boldsymbol{n}}$. Again, we assume homogeneous and orientation-independent excitation of the dye molecules. Considering light propagation parallel to the film normal in a nematic film with planar alignment, the two independent light modes are linear polarized parallel and perpendicular to the director $\hat{\boldsymbol{n}}$. We neglect multiple reflections at the film boundaries. Again we assume that each excited dye molecule emits into one of the two normal modes, and the respective emission rate is proportional to the projection of the transition dipole moment $\boldsymbol{d}$ on the respective polarization ($\hat{\boldsymbol{e}}_\parallel$ or $\hat{\boldsymbol{e}}_\perp$), and to the DOS ($\rho_\parallel$ or $\rho_\perp$) associated to the respective mode. The dispersion relations $k_{\parallel,\perp} = n_{\mathrm{e,o}}/(c\omega)$ of the two normal modes give densities of states $\rho_{\parallel,\perp} \sim n_{\mathrm{e,o}}$. Again performing the orientational average of the transition dipole moment, we obtain for the emission intensities polarized parallel and perpendicular to the director

$$I_\parallel \sim n_\mathrm{e}(2S_\mathrm{d} + 1), \tag{64}$$

$$I_\perp \sim n_\mathrm{o}(1 - S_\mathrm{d}). \tag{65}$$

Defining

$$r' = r n_\mathrm{o}/n_\mathrm{e}, \tag{66}$$

and using equations (64) and (65), we finally obtain

$$S_\mathrm{d} = \frac{r' - 1}{r' + 2}\,. \tag{67}$$

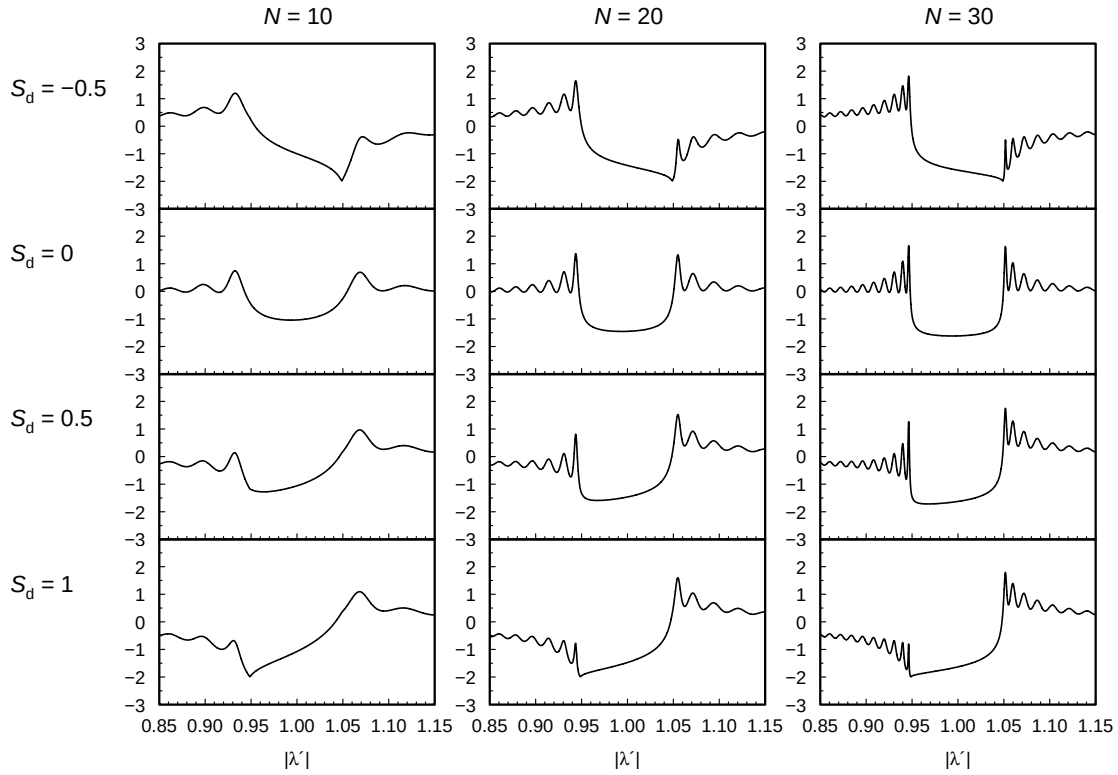

Fig. 9. Dissymmetry factor g_e for the fluorescence of a CLC film (taking into account multiple reflections), assuming $\alpha = 0.1$ and a lefthanded helix. The three columns correspond to the film thicknesses $N|p|$ as indicated at the top, the four rows correspond to the order parameter S_d indicated on the left.

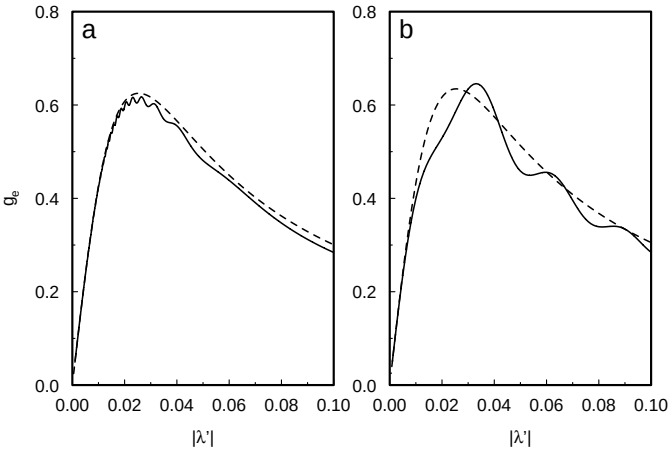

Fig. 10. Dissymmetry factor g_e at small wavelengths: according to the theory of Katsis *et al.* [13] (solid lines), and according to our theory (dashed lines), using $\alpha = 0.05$ and $S_d = 0.5$. (a): curves are calculated for a film with relative thickness $N = 5$; (b): calculated for film with thickness D, fixed emission wavelength λ, assuming $D\bar{n}/\lambda = 20$; variation of λ' corresponds to a variation of the pitch. Reflections at the film surface are neglected.

7 Limitations of the theory at short wavelengths

The dissymmetry factor for emission at small wavelengths ($\lambda' < \alpha$) has been studied both experimentally and theoretically by Chen's group [11,13]. According to their treatment, for wavelengths $\lambda' \ll p$, the emission of the dye molecules is essentially governed by the local quasi-nematic order, rather than the photonic properties of the film as a whole. For each quasi-nematic plane of the film, this results in incoherent linearly polarized emission contributions like in an ordinary nematic medium (Eqs. (64) and (65), again assuming homogeneous excitation of the dye molecules). For both emission contributions, the CLC layer between the emitting plane and the film surface acts as a polarizing device. The polarization of the light finally leaving the film depends on the distance of the emitting plane from the surface. Integration of the l-cp and r-cp emission contributions of all the emitting quasi-nematic sublayers gives the total l-cp and r-cp emission contributions of the film. The dissymmetry factor then shows undulations (solid lines in Fig. 10), their amplitude decreasing with increasing film thickness. While our theory qualitatively matches the Chen result, it doesn't reproduce the undulations in the dissymmetry factor due to the finite film thickness (in the framework of our theory, the dissymmetry factor is virtually independent of the film thickness at small wavelengths).

For small emission wavelengths $\lambda' < \alpha$, the model of Chen *et al.* has been found to be in excellent agreement with experimental results [13]. For wavelengths near or inside the stop band, their approach must fail, as it doesn't account for the drastic changes of the DOS. However, for a wide wavelength range we find quite good qualitative agreement of the dissymmetry factor obtained by the two theoretical approaches (Fig. 11, g_e calculated for a thick

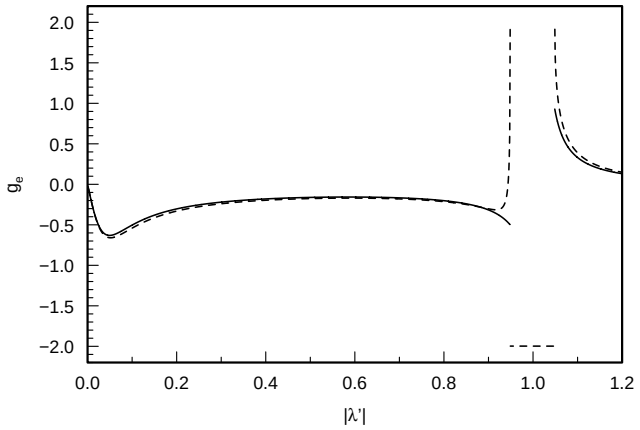

Fig. 11. Dissymmetry factor g_e of a thick cholesteric slab, calculated according to the theory of Katsis *et al.* [13] (solid line), and according to our theory (dashed line), using $\alpha = 0.1$ and $S_d = 0.5$.

CLC slab). Striking deviations occur close to the stop band, where the Chen theory doesn't reproduce the steep approach to the extremal value $|g_e| = 2$.

8 Experiment

To test our theory, we analyzed the fluorescence of two cholesteric samples, both of them being a mixture of a chiral and an achiral compound (Fig. 12). Sample 1 is a mixture of the nematic p-pentylphenyl-2 chloro-4-(pentylbenzoyloxy)-benzoate (69.2 wt.%) and the cholesteric cholesteryl nonanoate (30.8%), sample 2 is a mixture of the two diacrylates shown in Figure 2 (achiral component 95.94 wt.%, chiral component 4.06 wt.%). Both samples are doped with the laser dye 4-(dicyanomethylene)-2-methyl-6-(4-dimethylamino styryl)-4*H*-pyran (DCM, also shown in Fig. 12), which has a high quantum yield and shows excellent solubility in various liquid crystals. The dye contents of sample 1 and sample 2 are 0.37 and 0.21 weight-%, respectively. Sample films were prepared by filling ready-made ITO cells with buffed substrates (spacing ≈ 22 μm). They provide a well-defined director orientation at the film surfaces, thus enforcing an integer number of half-turns of the cholesteric helix. Sample 1 was chosen because of its high birefringence and the weak temperature sensitivity of the cholesteric pitch. Macroscopic uniform alignment was supported by annealing the film at 60 °C for several hours. Sample 2 is less well suited to prepare well ordered films, because annealing at elevated temperatures results in a chemical crosslinking reaction, which is accompanied with a change in density of the material and the formation of microscopic heterogeneities [8]. We have chosen sample 2 because of the small amount of the chiral component required to form a CLC showing selective reflection in the visible region. Thus, the cholesteric mixture, and the nematic phase formed by the achiral component alone, can be expected to have very similar nematic order parameters and refractive indices n_o, n_e, and both solvents provide an almost identical chemical environment for the dissolved DCM-molecules. Thus, a correct analysis of the fluorescence of the dye-doped cholesteric and nematic diacrylate should yield quite similar values of the order parameter S_d.

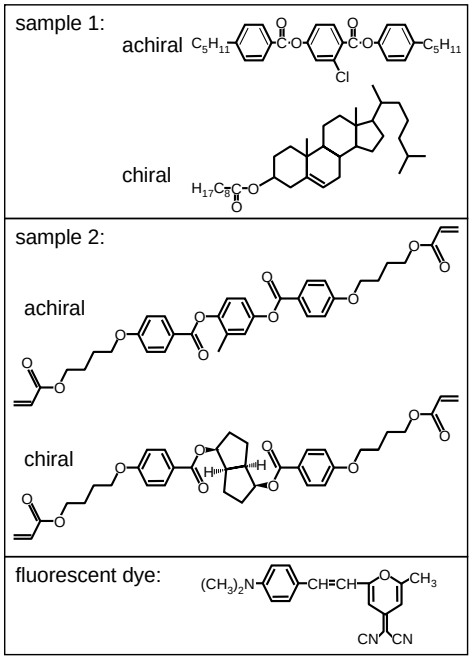

Fig. 12. Systems under investigation.

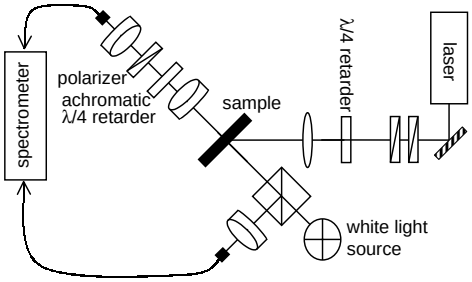

Fig. 13. Sketch of the experimental setup.

Due to small tilts of the substrates, usually there are small variations in the film thickness, resulting at a given surface orientation of the director in a variation of the local pitch; thus, if too large a film area is used for the excitation of fluorescence, the fine structure of the fluorescence spectrum resulting from the oscillations of the DOS can't be resolved properly. Therefore, we used for excitation a focused laser beam. Experiments were performed at room temperature, using the experimental setup sketched in Figure 13. Fluorescence is excited with a frequency-doubled cw Nd:YAG laser (COHERENT 532-200). The beam ($\lambda = 532$ nm) is strongly attenuated by two almost crossed polarizers, and then is converted into a circular polarized beam by means of a quarter-wavelength retarder. Finally, it passes a collecting lense ($f = 40$ mm, resulting in a focal spot with diameter ≈ 20 μm) and hits the sample film at an angle of incidence of 45°. The polarization's sense of rotation is chosen to be opposite to the handedness of sample's cholesteric twist; thus, inside the sample film, the excitation beam essentially resembles the normal mode with polarization $\hat{\boldsymbol{e}}_2$, which is virtually

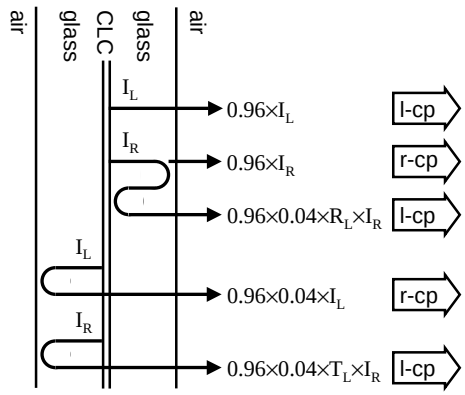

Fig. 14. Circularly polarized intensity contributions reaching the detector (assuming a sample with left-handed cholesteric helix, and $n_{\text{glass}} = 1.5$).

unaffected by the cholesteric medium. Due to the (almost) circular polarization of the beam inside the sample, the excitation probability is almost independent of the orientation of the individual dye molecules (we neglect the minor orientation dependence which is produced by the anisotropy of the local field, due to the optical anisotropy of the nematic planes).

The fluorescence light is parallelized by an achromatic lens, and passes a 'superachromatic' quarter-wavelength retarder (B. Halle Nachfolger Ltd) and a prism polarizer in a rotatable mount. Finally, it is coupled *via* fiber optics into a spectrometer (OceanOptics S2000). Reflection and transmission measurements were performed with a white light source providing an almost parallel incident beam (divergence $\approx 1°$) with a beam diameter 1.5 mm in the sample plane. Reflection measurements at normal incidence were accomplished with the help of a beam splitter cube positioned in the path of the incident beam. The two spectrometer channels for fluorescence and reflection measurements have resolutions of 0.5 nm and 1.5 nm, respectively. The spectra were corrected for the wavelength- and polarization-dependent sensitivity of the spectrometer.

For a correct quantitative evaluation of the cp intensity contributions reaching the detector, we have to consider the effects due to reflections at the glass-air interfaces of the sample cell. Small parts of the two cp emission components are reflected at the glass-air interface, thereby reversing the handedness of their respective polarizations. This results in a mixing of the l-cp and r-cp emission components I_{L}, I_{R}. Assuming a sample with left-handed cholesteric helix, a back-reflected r-cp beam passes the CLC film virtually unimpeded, while a l-cp beam is partially reflected by the CLC film. In contrast to reflection at the glass-air interface, the polarization's handedness is *not* reversed by reflection at the CLC-film [1,2]. The contributions to the detected cp intensities $I_{\text{L,tot}}$, $I_{\text{R,tot}}$ are shown in Figure 14. For simplicity, we only consider corrections of the first order in the reflectivity R of the glass-air interface (for $n_{\text{glass}} = 1.5$, $R = 0.04$). The transmittance and reflectivity of the CLC film for l-cp light are denoted in the figure by T_{L} and R_{L}. For the total l-cp and r-cp intensity contributions finally leaving the sample cell, we

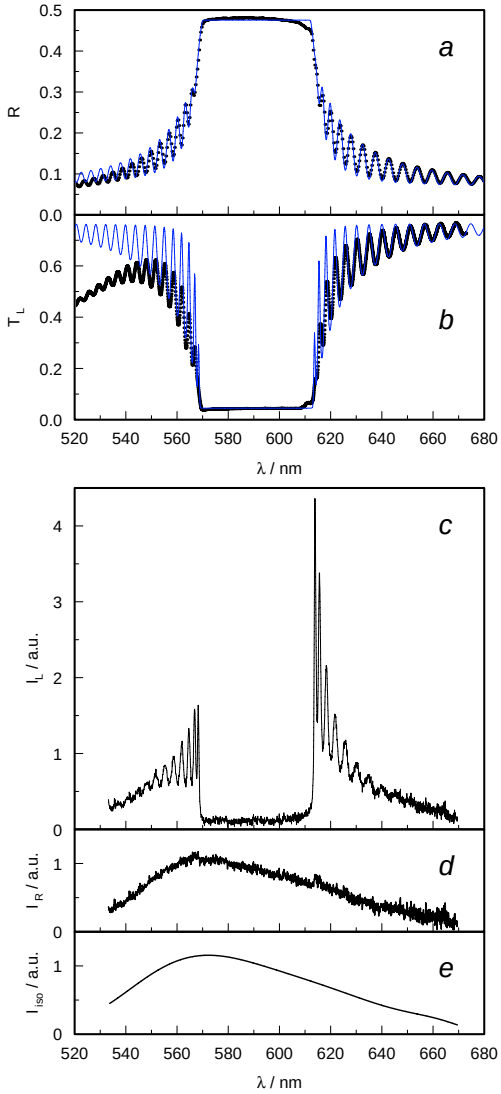

Fig. 15. Optical characterization and fluorescence of sample 1. Top: reflectivity (a) and l-cp transmission (b); dots and solid curves represent experimental results and fitted theoretical curves, respectively. Bottom: fluorescence spectra: l-cp emission (c) and r-cp emission (d); and emission in the isotropic phase (e).

obtain (using $T_L + R_L = 1$)

$$I_{\text{L,tot}} = 0.96 \times (I_{\text{L}} + 0.04 I_{\text{R}}), \tag{68}$$

$$I_{\text{R,tot}} = 0.96 \times (0.04 I_{\text{L}} + I_{\text{R}}). \tag{69}$$

The sum of these two intensities gives

$$I_{\text{L,tot}} + I_{\text{R,tot}} = 0.9984 \times (I_{\text{L}} + I_{\text{R}}), \tag{70}$$

so the error due to neglecting higher-order reflections is negligible (0.16%).

9 Experimental results and discussion

In Figures 15a and b, the reflection and transmission curves for sample 1 are shown. The almost perfect cholesteric order within the illuminated spot results in a

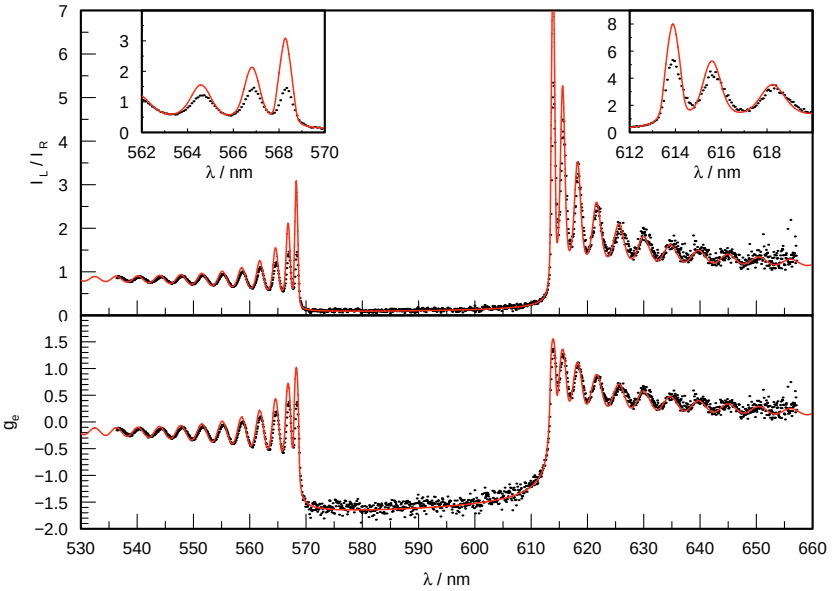

Fig. 16. Sample 1: ratio of l-cp and r-cp emission component of the fluorescence (top), and dissymmetry factor g_e (bottom). Experimental results and theoretical curves are represented as dots and solid lines, respectively. Insets in the top figure show the peaks near the band edges.

clear-cut stop band and pronounced interference fringes. The drop in transmittance at short wavelengths is due to the absorption of the dye. The reflectivity curve is excellently matched by the fitted theoretical curve [2] (convoluted with the resolution of the spectrometer) also plotted in Figure 15a. The parameters thus derived are $|p|\bar{n} = 591.4\,\text{nm}$, $\alpha = 0.0746$, and $N = 58.5$. In Figures 15c and d, we present the l-cp and r-cp emission components of the fluorescence spectrum (obtained at the same sample spot we used for the reflection- and transmission measurement). The CLC under investigation forms a left-handed cholesteric helix, and – as to be expected – only the l-cp emission component is strongly affected by the cholesteric medium: almost zero emission inside the selective stop band, strongly enhanced emission at the long-wavelength band edge, and strong oscillations near the band edges. The r-cp emission component essentially resembles the fluorescence spectrum obtained in the isotropic phase of the CLC (Fig. 15e).

The ratio I_L/I_R of the l-cp and r-cp emission component, and the dissymmetry factor g_e are shown in Figure 16. Although both quantities contain equivalent information, we show both of them: the ratio I_L/I_R gives a qualitative impression of the DOS of the normal mode $\boldsymbol{E}_1$, and the dissymmetry factor g_e illustrates the drastic wavelength dependence of the polarization of the emitted light. Also included in the figure as solid lines are the respective curves calculated according to our theory (again we have taken into account the spectrometer's resolution); a best fit of the data is obtained for the cholesteric parameters $|p|\bar{n} = 591.46$ nm, $\alpha = 0.0752$, and $N = 59$ (in excellent agreement with the results derived from the reflection curve), and order parameter $S_\text{d} = 0.42$, indicating a rather strong alignment of the dye's transition dipole moment for emission parallel to the director. Although the assumption of a constant order parameter S_d can't be expected to be strictly true, the overall agreement of the experimental and theoretical results is excellent. There are some deviations: the measured intensity peaks near the band edges are less pronounced than predicted by theory (see insets in Fig. 16). Our calculation of the DOS is based on the assumption of a perfect cholesteric order. However, there might exist static distortions due to defects, and due the inhomogeneous heating of the sample by the strongly focussed excitation beam. Besides, there exist long range thermal fluctuations of the molecular alignment; they disturb the periodicity of the structure [18,19], give rise to random light scattering and thus reduce the resonator quality of the CLC film. Deviations near the short-wavelength edge of the selective stop band may be partially due to re-absorption of the emitted light. A small contribution to the observed discrepancies may derive from the fact, that the excitation of the chromophores is not exactly homogeneous along the film normal.

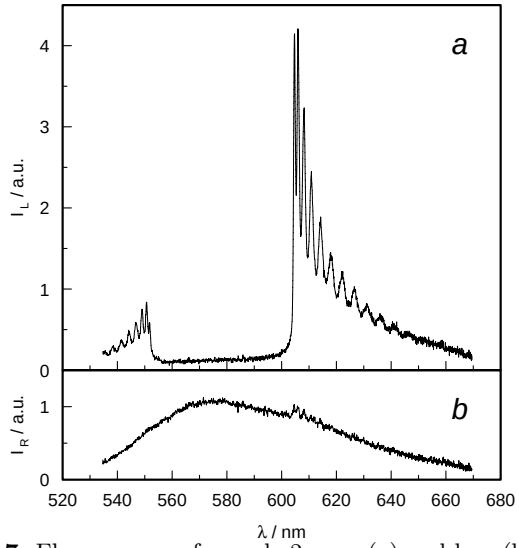

Fig. 17. Fluorescence of sample 2: r-cp (a) and l-cp (b) emission contributions.

In Figure 17, the l-cp and r-cp emission components of sample 2 are shown. Since sample 2 forms a right-handed cholesteric helix, now the r-cp emission

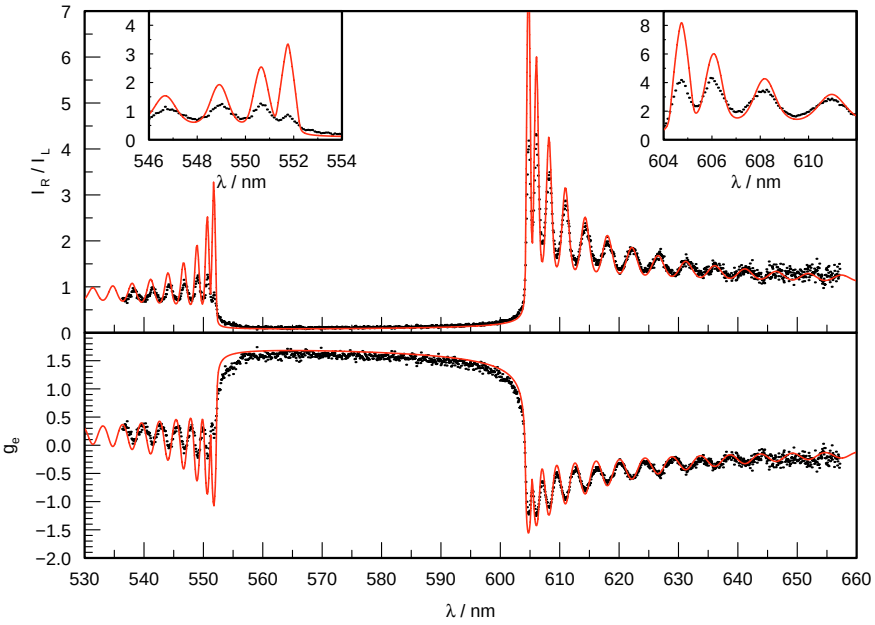

Fig. 18. Sample 2: ratio of r-cp and l-cp emission component of the fluorescence (top), and dissymmetry factor g (bottom). Experimental results and theoretical curves are represented as dots and solid lines, respectively. Insets in the top figure show the peaks near the band edges.

component is strongly affected by the cholesteric medium. As outlined above, sample 2 isn't ordered as well as sample 1, as revealed by the less pronounced emission peaks (especially the two peaks framing the stop band are strongly attenuated). The ratio of the r-cp and l-cp emission contributions, and the dissymmetry factor g_e are shown in Figure 18. Again, there is fair agreement of our model and the experimental result, with parameters $p\bar{n} = 578.8$ nm, $\alpha = 0.090$, $N = 61.5$, and $S_d = 0.38$. The S_d – value is very similar to the result obtained for sample 1. In general one has to expect varying order parameters S_d in different cholesteric solvents: the alignment of the dye molecules depends on the solvent's chemical constitution and on the nematic order parameter. Additionally, in the case of DCM there is a well-known dependence of the equilibrium conformation of the DCM molecule on the solvent, which affects the emission characteristics [20].

For comparison, we studied the fluorescence of a dye-doped nematic film formed by the achiral compound also used for sample 2. The two linear polarized emission contributions $I_\parallel$, $I_\perp$, with polarization parallel and perpendicular to the nematic director, are shown in Figure 19a. The small ripples of the $I_\parallel$ – spectrum may be assigned to oscillations of the DOS due to Fabry-Perot interference. The refractive indices n_o, n_e of sample 2 and the nematic film can be expected to be almost identical. To determine S_d from the emission ratio $I_\parallel/I_\perp$ of the nematic sample according to equation (67), we need the ratio of the refractive indices n_o/n_e; it can be calculated from the parameter α of sample 2 according to

$$n_o/n_e = [(1-\alpha)/(1+\alpha)]^{1/2}, \qquad (71)$$

and we get $n_o/n_e = 0.914$. Using equation (67), we finally obtain S_d as a function of emission wavelength (Fig. 19b).

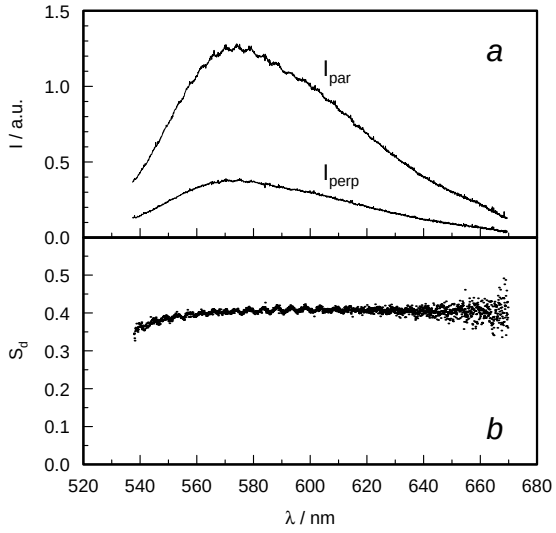

Fig. 19. Nematic sample: linear polarized emission contributions (a), and order parameter S_d (b).

The result is almost constant (except near the excitation wavelength). Within the experimental accuracy, the mean value $S_d \approx 0.41$ is in excellent agreement with the result derived from the fluorescence of the CLC sample 2, as to be expected due to the almost identical chemical constitution of the two solvents.

10 Conclusions

In this paper, we have discussed the changes in fluorescence of a dye-doped CLC film on transition from the

isotropic to the cholesteric phase, considering emission parallel to the cholesteric helix. Assuming a homogeneous distribution and excitation of the fluorescent molecules in the film, and neglecting re-absorption of the emitted light, we have derived a theoretical description of the changes in the fluorescence intensity and polarization for emission parallel to the film normal. The salient features of fluorescence spectra of dye-doped CLC films – reduced intensity inside the stop band, enhanced fluorescence at the band edges, oscillations in the vicinity of the stop band, and a dominant circularly polarized emission contribution – can be well understood in the framework of our theory. Agreement of our model with experimental results is excellent; the values obtained for the model parameters are in agreement with the results of complementary measurements: For sample 1, the values of the optical and structural parameters ($\bar{n}p$, α, N) are consistent with those obtained by a reflectivity measurement, and for sample 2, the value of the order parameter S_d is in agreement with the value obtained using a nematic solvent with very similar chemical constitution.

From our results, several conclusions can be drawn concerning the observed laser emission of dye-doped CLC films. The sharp peaks of the DOS in the vicinity of the stop band mark the resonance frequencies which may be available for laser emission. The two sequences of resonant peaks near the two band edges are roughly symmetric (*cf.* Fig. 3), the resonances near the short-wavelength edge being slightly more pronounced. Thus, apparently both band edges are equally well suited for laser emission (neglecting the fact, that in general population inversion is more easily achieved at longer wavelengths). However, one has to take into account the alignment of the transition dipole moment for emission, $\hat{\boldsymbol{d}}$, of the dye molecules with respect to the polarization $\hat{\boldsymbol{e}}_1$ of the resonant mode. The average $\langle|\hat{\boldsymbol{e}}_1^* \cdot \hat{\boldsymbol{d}}|^2\rangle$ (Fig. 5) of course not only governs the effect of the order parameter S_d on spontaneous emission, but on stimulated emission as well: for positive order parameters S_d, stimulated emission preferentially takes place at the resonance frequencies near the long-wavelength edge of the stop band, and for negative S_d, the resonances near the long-wavelength edge are preferred. Indeed, both the dye-doped CLC sample 1, as well as a highly crosslinked cholesteric polymer network formed by the diacrylate monomers we used for sample 2, show laser emission at the long-wavelength edge of the stop band [8], as to be expected for a system with positive order parameter S_d.

Thanks are due to the *Fonds der Chemischen Industrie* and the *Deutsche Forschungsgemeinschaft* (SFB 428) for financial support, as well as to BASF AG (Ludwigshafen) for providing the diacrylate monomers.

Appendix

Here we list the derivatives of basic optical quantities which are needed for the calculation of the DOS. For waves with polarization $\hat{\boldsymbol{e}}_2$ at all wavelengths, and for waves with polarization $\hat{\boldsymbol{e}}_1$ outside the stop band, they read

$$\frac{\mathrm{d}\lambda'}{\mathrm{d}\omega} = -\frac{2\pi c}{\bar{n}p}\omega^{-2} = -\frac{\bar{n}p}{2\pi c}\lambda'^2, \tag{A.1}$$

$$\frac{\mathrm{d}m'_{1,2}}{\mathrm{d}\lambda'} = \left(1 \mp \frac{2}{\sqrt{4\lambda'^2+\alpha^2}}\right)\frac{\lambda'}{m'_{1,2}}, \tag{A.2}$$

$$\frac{\mathrm{d}k_i}{\mathrm{d}\lambda'} = 2\pi\left(\frac{1}{\lambda'}\frac{\mathrm{d}m'_i}{\mathrm{d}\lambda'} - \frac{m'_i}{\lambda'^2}\right), \tag{A.3}$$

$$\frac{\partial f_i}{\partial \lambda'} = \left(m'_i - \frac{1-\alpha}{m'_i}\right)\frac{1}{2\lambda'^2} - \frac{1}{2m'_i}, \tag{A.4}$$

$$\frac{\partial f_i}{\partial m'_i} = \left(\lambda' - \frac{1-\alpha}{\lambda'}\right)\frac{1}{2m'^2_i} - \frac{1}{2\lambda'}, \tag{A.5}$$

$$\frac{\mathrm{d}f_i}{\mathrm{d}\lambda'} = \frac{\partial f_i}{\partial \lambda'} + \frac{\partial f_i}{\partial m'_i}\frac{\mathrm{d}m'_i}{\mathrm{d}\lambda'}, \tag{A.6}$$

$$\frac{\mathrm{d}q_i}{\mathrm{d}\lambda'} = f_i + \lambda'\frac{\mathrm{d}f_i}{\mathrm{d}\lambda'} + \frac{\mathrm{d}m'_i}{\mathrm{d}\lambda'}, \tag{A.7}$$

$$\frac{\mathrm{d}r_i}{\mathrm{d}\lambda'} = \frac{2}{(1+q_i)^2}\frac{\mathrm{d}q_i}{\mathrm{d}\lambda'}\,. \tag{A.8}$$

For the calculation of the DOS of the wave with polarization $\hat{\boldsymbol{e}}_1$ inside the stop band, we write the now imaginary quantities k'_1, m'_1, f_1 and q_1 in the form $k'_1 = \mathrm{i}\tilde{k}'_1$, $m'_1 = \mathrm{i}\tilde{m}'_1$, $f_1 = \mathrm{i}\tilde{f}_1$, $q_1 = \mathrm{i}\tilde{q}_1$. The derivatives read

$$\frac{\mathrm{d}\tilde{m}'_1}{\mathrm{d}\lambda'} = -1 + \frac{2}{\sqrt{4\lambda'^2+\alpha^2}}\frac{\lambda'}{\tilde{m}'_1}, \tag{A.9}$$

$$\frac{\partial \tilde{f}_1}{\partial \lambda'} = \left(\tilde{m}'_1 + \frac{1-\alpha}{\tilde{m}'_1}\right)\frac{1}{2\lambda'^2} + \frac{1}{2\tilde{m}'_1}, \tag{A.10}$$

$$\frac{\partial \tilde{f}_1}{\partial \tilde{m}'_1} = \left(\frac{1-\alpha}{\lambda'} - \lambda'\right)\frac{1}{2\tilde{m}'^2_1} - \frac{1}{2\lambda'}, \tag{A.11}$$

$$\frac{\mathrm{d}\tilde{f}_1}{\mathrm{d}\lambda'} = \frac{\partial \tilde{f}_1}{\partial \lambda'} + \frac{\partial \tilde{f}_1}{\partial \tilde{m}'_1}\frac{\mathrm{d}\tilde{m}'_1}{\mathrm{d}\lambda'}, \tag{A.12}$$

$$\frac{\mathrm{d}\tilde{q}_1}{\mathrm{d}\lambda'} = \tilde{f}_1 + \lambda'\frac{\mathrm{d}\tilde{f}_1}{\mathrm{d}\lambda'} + \frac{\mathrm{d}\tilde{m}'_1}{\mathrm{d}\lambda'}\,. \tag{A.13}$$

Inside the stop band, the derivatives of the real and imaginary part of the reflection coefficient $r_1 = r_\mathrm{a} + \mathrm{i}r_\mathrm{b}$ read

$$\frac{\mathrm{d}r_\mathrm{a}}{\mathrm{d}\lambda'} = \frac{4}{(1+\tilde{q}_1^2)^2}\frac{\mathrm{d}\tilde{q}_1}{\mathrm{d}\lambda'}, \tag{A.14}$$

$$\frac{\mathrm{d}r_\mathrm{b}}{\mathrm{d}\lambda'} = \frac{2(1-\tilde{q}_1^2)}{(1+\tilde{q}_1^2)^2}\frac{\mathrm{d}\tilde{q}_1}{\mathrm{d}\lambda'}\,. \tag{A.15}$$

The derivatives of the factors A, B, C and D (Eqs. (42–45)) read

$$\frac{\mathrm{d}A}{\mathrm{d}\lambda'} = \frac{\mathrm{d}r_\mathrm{a}}{\mathrm{d}\lambda'} + \frac{\mathrm{d}\tilde{q}_1}{\mathrm{d}\lambda'} r_\mathrm{b} + \tilde{q}_1 \frac{\mathrm{d}r_\mathrm{b}}{\mathrm{d}\lambda'}, \tag{A.16}$$

$$\frac{\mathrm{d}B}{\mathrm{d}\lambda'} = \frac{\mathrm{d}r_\mathrm{b}}{\mathrm{d}\lambda'} - (1 + r_\mathrm{a}) \frac{\mathrm{d}\tilde{q}_1}{\mathrm{d}\lambda'} - \tilde{q}_1 \frac{\mathrm{d}r_\mathrm{a}}{\mathrm{d}\lambda'}, \tag{A.17}$$

$$\frac{\mathrm{d}C}{\mathrm{d}\lambda'} = \left[r_\mathrm{b} \frac{\mathrm{d}r_\mathrm{b}}{\mathrm{d}\lambda'} - r_\mathrm{a} \frac{\mathrm{d}r_\mathrm{a}}{\mathrm{d}\lambda'} + N(r_\mathrm{a}^2 - r_\mathrm{b}^2) \frac{\mathrm{d}\tilde{k}_1'}{\mathrm{d}\lambda'} \right] \times 2 \exp\left(-2\tilde{k}_1' N\right), \tag{A.18}$$

$$\frac{\mathrm{d}D}{\mathrm{d}\lambda'} = \left(\frac{\mathrm{d}r_\mathrm{a}}{\mathrm{d}\lambda'} r_\mathrm{b} + r_\mathrm{a} \frac{\mathrm{d}r_\mathrm{b}}{\mathrm{d}\lambda'} - N \frac{\mathrm{d}\tilde{k}_1'}{\mathrm{d}\lambda'} \right) \times 2 \exp\left(-2\tilde{k}_1' N\right). \tag{A.19}$$

References

1. P.G. de Gennes, J. Prost, *The Physics of Liquid Crystals*, 2nd edn. (Clarendon Press, Oxford 1993)
2. H. de Vries, Acta Cryst. **4**, 219 (1951)
3. I.P. Il'chishin, E.A. Tikhonov, V.G. Tishchenko, M.T. Shpak, JETP Lett. **32**, 24 (1980)
4. I.P. Il'chishin, A.Y. Vakhin, Mol. Cryst. Liq. Cryst. **265**, 687 (1995)
5. V.I. Kopp, B. Fan, H.K.M. Vithana, A.Z. Genack, Opt. Lett. **23**, 1707 (1998)
6. E. Alvarez, M. He, A.F. Muñoz, P. Palffy-Muhoray, S.V. Serak, B. Taheri, R. Twieg, Mol. Cryst. Liq. Cryst. **369**, 75 (2001)
7. H. Finkelmann, S.T. Kim, A. Muñoz, P. Palffy-Muhoray, B. Taheri, Adv. Mater. **13**, 1069 (2001)
8. J. Schmidtke, W. Stille, H. Finkelmann, S.T. Kim, Adv. Mater. **14**, 746 (2002)
9. P. Pollmann, K.-J. Mainusch, H. Stegemeyer, Z. Physik. Chem. (NF) **103**, 295 (1976)
10. B.M. Conger, J.C. Mastrangelo, S.H. Chen, Macromolecules **30**, 4049 (1997)
11. H. Shi, B.M. Conger, D. Katsis, S.H. Chen, Liq. Cryst. **24**, 163 (1998)
12. B.M. Conger, D. Katsis, J.C. Mastrangelo, S.H. Chen, J. Phys. Chem. A **102**, 9213 (1998)
13. D. Katsis, A.W. Schmid, S.H. Chen, Liq. Cryst. **26**, 181 (1999)
14. S.H. Chen, D. Katsis, A.W. Schmid, J.C. Mastrangelo, T. Tsutsui, T.N. Blanton, Nature **397**, 506 (1999)
15. M. Voigt, M. Chambers, M. Grell, Chem. Phys. Lett. **347**, 173 (2001)
16. M.D. Tocci, M. Scalora, M.J. Bloemer, J.P. Dowling, C.M. Bowden, Phys. Rev. A **53**, 2799 (1996)
17. J.M. Bendickson, J.P. Dowling, M. Scalora, Phys. Rev. E **53**, 4107 (1996)
18. C. Fan, L. Kramer, M.J. Stephen, Phys. Rev. A **2**, 2482 (1970)
19. M.S. Giridhar, K.A. Suresh, Eur. Phys. J. E **7**, 167 (2002)
20. J.M. Drake, M.L. Lesiecki, D.M. Camaioni, Chem. Phys. Lett. **113**, 530 (1985)